Comparative Studies on Corrosion Protection Properties of Polyimide-Silica and Polyimide-Clay Composite Materials

Tsao-Cheng Huang,[1] Chi-Fa Hsieh,[2] Tzu-Chun Yeh,[1] Cheug-Ling Lai,[1] Mei-Hui Tsai,[3] Jui-Ming Yeh[1]

[1]*Department of Chemistry, Center for Nanotechnology at CYCU, Chung-Yuan Christian University, Chung Li, Taiwan 32023, Republic of China*
[2]*Chemical System Research Division, Chuang Shan Institute of Science and Technology, Tao-Yuan, Taiwan 32599, Republic of China*
[3]*Department of Chemical and Materials Engineering, National Chin-Yi University of Technology, Taichung, Taiwan 411, Republic of China*

Received 21 December 2009; accepted 16 April 2010
DOI 10.1002/app.32669
Published online 27 July 2010 in Wiley Online Library (wileyonlinelibrary.com).

ABSTRACT: Comparative studies on corrosion protection properties of polyimide-silica-clay composites were studied in this article. A series of polyimide-silica (PIS), polyimide-clay (PIC), and polyimide-silica-clay composites (PISC) materials, consisting of an organo-soluble polyimide (ODA-BSAA) matrix, inorganic silica particles prepared through the sol–gel reaction of tetraethyl orthosilicate (TEOS) and dispersed nanolayers of inorganic montmorillonite clay, were successfully prepared by solution dispersion technique. Then, all samples were characterized by FTIR, powder X-ray diffraction patterns, transmission electron microscopy, and ^{29}Si solid-state NMR. The main focus of this article is the comparison of the corrosion protection properties of PIS, PIC, and PISC composite materials. Normally, the aspect ratio of clay is higher than silica. Superior dispersion of clay platelets into a polymer matrix may effectively increase the length of diffusion pathways for oxygen and water. The effects of the materials composition on the corrosion protection performance, gas barrier, and optical properties, in the form of both coating and film, were also studied by electrochemical corrosion measurements (e.g., corrosion potential, polarization resistance, corrosion current, and impedance spectroscopy), gas permeability analysis, and UV-visible transmission spectroscopy. © 2010 Wiley Periodicals, Inc. J Appl Polym Sci 119: 548–557, 2011

Key words: polyimide; organo-soluble; sol–gel; corrosion

INTRODUCTION

Recently, composite materials based on organic polymers and inorganic clay minerals including the silicate layers have evoked great academic and industrial interest. In literature reviews, polymer-clay composite materials have many developed functional properties such as thermal,[1] mechanical,[2] barrier,[3,4] and even flame-retardant properties[5] compared to traditional composites. It is probably owing to the unique phase morphology by the formation of layer intercalation or exfoliation structure, which maximizes interfacial contact between the organic and inorganic phases and promotes interfacial properties. In the past, Yeh et. al.[6–8] had demonstrated that the incorporation of organophilic clay platelets into polymer matrix, in the form of organic-based coatings, may effectively enhance the corrosion protection of polymers on metallic surface. It is due to the good dispersion of platelike-shape clay platelets into polymer matrix, which may effectively increase the length of diffusion pathways for oxygen and water. Also, it may decrease the permeability of coatings.

Apart from clay, another important material with this advantage is the SiO_2 particle. Since 1970s, the sol–gel process has been used for the deposition of inorganic minerals *in situ* in an organic polymer matrix. Polymers containing SiO_2 particle usually with special properties and consequently can be used in many fields such as plastics, rubbers, coatings, and inks. In this study, we prepared inorganic silica particles through the sol–gel reaction of tetraethyl orthosilicate (TEOS). The starting materials for the sol–gel process are metal alkoxides M(OR)n and a small amount of acid or base as a catalyst.[9] A polymer-silica has been used commonly to prepare creamer coatings and also protect the metal surface from

Correspondence to: J.-M. Yeh (juiming@cycu.edu.tw).
Contract grant sponsor: National Science Council (NSC); contract grant number: NSC 98-2113-M-033 -001 -MY3.
Contract grant sponsor: Chung Yuan Christian University, Taiwan; contract grant number: CYCU-97-CR-CH.
Contract grant sponsor: Ministry of Education, Taiwan, R.O.C (Center-of-Excellence Program on Membrane Technology).

corrosion.[10–12] In the past decades, several reports have shown the corrosion protection of metals by sol–gel derived organic–inorganic hybrids.[13–15]

Aromatic polyimides (PIs) are generally classified as thermally stable polymers due to the excellent mechanical strength and the thermal stability among many engineering polymers.[16–20] Hence, improving the anticorrosion properties of polyimide composites is an important issue. This article reports in a series of PIS, PIC, and PISC materials, consisting of 4,4′-(4,4′-isopropylidene-diphenoxy)-bis(phthalic anhydride) and 4,4′-oxdianiline (ODA-BSAA) polyimide, silica particles, and layered montmorillonite (MMT) clay, were successfully prepared by a solution dispersion technique. The prepared materials were characterized by FTIR, powder XRD, ^{29}Si solid-state NMR, and TEM. The PIS, PIC, and PISC materials in the form of a coating loaded with low content on CRS coupons had different effects in anticorrosion efficiency by measuring in 5 wt % aqueous NaCl electrolyte. The effect of material composition on the molecular barrier of PIS, PIC, and PISC materials was also investigated by gas permeability analysis and ultraviolet-visible transmission spectroscopy.

MATERIALS AND METHODS

Materials and instrumentations

4,4′-Oxydianiline (ODA; Fluka, Buchs, Switzerland), 1-methyl-2-pyrrolidone (NMP, 99.7%; Tedia, Fairfield, OH), *N*,*N*-Dimethylacetamide (DMAc; Mallinckrodt/Baker, Paris, KY), Hexadecyltrimethylammonium bromide [HTAB; $CH_3(CH_2)_{15}N(CH_3)_3^+Br^-$, 99.9% Acros Organics, Morris Plains, NJ], Melamine (Lancaster. 99%), and 4,4′-(4,4′-Isopropylidene diphenoxy)-bis(phthalic anhydride) (BSAA, 97%, Aldrich, Milwaukee, WI) were used as received without further purification. Montmorillonite (MMT) clay, having a cation-exchange capacity (CEC) value of 116 mequiv/100 g and a unit cell formula $Na^+_{0.31}[Al_{1.67}Mg_{0.33}]\ Si_4O_{10}(OH)^{\bullet}_2\ 5.8H_2O$, was provided by Industrial Technology Research Institute (ITRI), Taiwan. Electrochemical measurements of sample-coated cold-rolled steel (CRS) coupons were performed on a VoltaLab 21 and VoltaLab 40 potentiostat/galvanostat (Radiometer Analytical/London Scientific, Ontario, Canada) in a standard corrosion cell equipped with two graphiterod counterelectrodes and a saturated calomel electrode (SCE) as well as the working electrode. FTIR spectra were recorded on pressed KBr pellets using a Nicolet model Magna 550 and a Perkin Elmer Spectrum 2000 Explorer (for ATR studies) FTIR spectrometer. The ^{29}Si solid-state NMR is obtained using a BRUKER AVANCE 400 and $d_1 = 200$ s, $P_1 = 3$ μs. Wide-angle X-ray diffraction study of the samples was performed on a D/MAX-3C OD-2988N X-ray diffractometer (Rigaku, Tokoy, Japan) with cooper target and Ni filter at a scanning rate of 4°/min. The samples for transmission electron microscopy (TEM) study were first prepared by filling epoxy resin capsules with the powder of PISC materials followed by curing the epoxy resin at 100°C for 24 h in a vacuum oven. Then the cured epoxy resins, containing PISC materials, were microtomed with an Ultracut-E apparatus (Reichert-Jung GmbH, Arnsberg, Germany) into 60–90 nm thick slices. Subsequently, one layer of carbon, about 10 nm thick, was deposited on these slices on 100-mesh copper nets for TEM observations on a JEOL-200FX (JEOL, Tokyo, Japan) with an acceleration voltage of 120 kV. A model GTR 10 gas permeability analyzer (Yanagimoto Co., Kyoto, Japan) was used to carry out the permeation experiment of oxygen gas and water vapor. UV-visible transmission spectra were obtained using a U-2000 UV-visible spectrometer (Hitachi, Osaka, Japan).

Synthesis of soluble polyimide derived from ODA/BSAA

A one-step method was used in this study. A typical procedure to prepare the organo-soluble polyimide (PI) is given as follows: BSAA (0.025 mol, 13.0 g) was added to 54.0 g of DMAc (denoted beaker A) at room temperature, with continuous stirring, for 30 min. A separate solution containing ODA (0.025 mol, 5.0 g) in another 30.0 g of DMAc (denoted beaker B) was prepared under mechanical stirring. After stirring for 30 min, both were subsequently mixed. The as-prepared mixture was then stirred for additional 48 h at 165°C under nitrogen gas purge. After cooling, the resultant polymer solution was poured slowly with stirring into 500 mL of warm water. The precipitated polymer was collected by filtration, washed thoroughly with hot methanol, and dried to give a quantitative yield of the ODA/BSAA polyimide.[21,22]

Preparation of organophilic clay

Typically, 5 g of MMT clay with a CEC value of 98 mEq $(100\ g)^{-1}$ was stirred in 600 mL of distilled water (beaker A) at room temperature overnight. A separate solution containing 0.8 g of intercalating agent (CTAB) in 30 mL of distilled water (beaker B) was prepared with the aid of magnetic stirring and the addition of a 1.0 mol L^{-1} HCl aqueous solution to adjust the pH value to 3–4. After stirring for 3 h, the protonated amino acid solution (beaker B) was added to the MMT suspension (beaker A) at a rate of ~ 5 mL min^{-1} with vigorous stirring. The mixture was stirred overnight at room temperature. A separate solution containing 0.49 g of intercalating agent

(melamine) in 30 mL of distilled water (beaker C) was prepared with the aid of magnetic stirring and the addition of a 15 mL 1.0 mol L^{-1} HCl aqueous solution into a ODA solution. After stirring for 3 h, the protonated amino acid solution (beaker C) was added to the MMT suspension (beaker A + B) at a rate of $\sim$ 5 mL min^{-1} with vigorous stirring. The mixture was stirred overnight at room temperature. The organophilic MMT was recovered using ultracentrifugation (9000 rpm, 30 min) and filtering in a Buchner funnel. Organophilic MMT purification was achieved by washing and filtering at least four times to remove any excess ammonium ions.[6–8]

Preparation of polyimide/clay, polyimide/silica and polyimide/clay/silica composites

A procedure of preparing the 5 wt % clay of PIC is given as follows: A polymer solution was made by dissolving 0.2 g of ODA/BSAA sample in NMP 3.29 mL. An amount of organophilic clay (0.0105 g) was stirred in NMP 3.29 mL at room temperature for 24 h. The clay dispersion was then added to the polyimide solution, and the mixture was stirred vigorously at ambient temperature for 48 h, then the PIC5% solution was obtained.

A procedure of preparing the 5 wt % silica of PIS is given as follows: A polymer solution containing 0.2 g ODA/BSAA dissolving in NMP 3.29 mL, and the TEOS (0.0364 g) was added into polymer solution and the addition of a 0.0126 g HCl aqueous solution under magnetic stirring for 6 h at room temperature, then the PIS5% solution was obtained. The resulting PIS5% solution was cast onto a glass plate and placed in an oven to form PIS5% composites.

A procedure of preparing the 2.5 wt % clay and 2.5 wt % silica of PISC is given as follows: A polymer solution was made by dissolving 0.2 g of ODA/BSAA sample in NMP 3.29 mL. An amount of organophilic clay (0.0053 g) was stirred in NMP 3.29 mL at room temperature for 24 h. The clay dispersion was then added to the polyimide solution, and the mixture was stirred vigorously at room temperature for 48 h, then the PI/clay solution was obtained. TEOS (0.0184 g) was added into 0.064 g of acidic water under magnetic stirring for 2 h at room temperature, both were subsequently mixed and stirred for 4 h at room temperature. The PISC2.5% solution was obtained, as showed in Scheme 1.

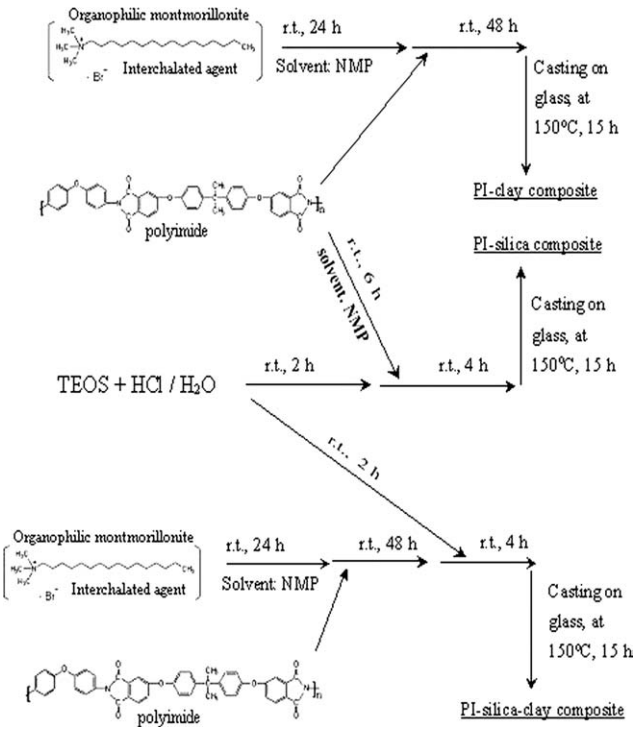

Scheme 1 Flowchart for the preparation of polyimide-silica-clay composite.

Preparation of coatings and electrochemical measurements

The PISC solution were cast drop onto the cold-rolled steel (CRS) coupons (1.0 × 1.0 cm) followed by drying in air for 24 h at 40°C to give coatings of about 30 ± 2 μm in thickness, measured by a digimatic micrometer (Mitutoyo, Tokyo, Japan). The coating ability of PISC solution on CRS is similar to that of bulk polyimide. The coated and uncoated coupons were then mounted on the working electrode so that only the coated side of the coupon was in direct contact with the electrolyte. The edges of the coupons were sealed with superfast epoxy cement. All the electrochemical measurements of corrosion potential, polarization resistance, and corrosion current were performed on a VoltaLab model 21 potentiostat/galvanostat and repeated at least three times. The electrolyte was NaCl (5 wt %) aqueous solution. The open circuit potential (OCP) at the equilibrium state of the system was recorded as the corrosion potential (E_{corr} in V versus SEC). The polarization resistance (R_p in Ω/cm^2) was measured by sweeping the applied potential from 20 mV below to 20 mV above the E_{corr} at a scan rate of 500 mV/min and by recording the corresponding current change. The R_p value was obtained from the slope of the potential-current plot. The Tafel plots were obtained by the scanning potential from 250 mV below to 250 mV above the E_{corr} at a scan rate of 10 mV/min. The corrosion current (I_{corr}) was determined through superimposing a straight line along the linear portion of the cathodic or anodic curve and extrapolating it through E_{corr}. The corrosion rate (R_{corr}, in milli-inches per year, MPY) was calculated from the following equation:

$$R_{corr}\ (\mathrm{MPY}) = [0.13 \times I_{corr}(\mathrm{E.W.})]/[A \cdot d]$$

where E.W. is the equivalent weight (in g/eq.) of the CRS, A is the area (cm^2) of the coated CRS, and d is the density (g/cm^3) of the CRS. A VoltaLab 40 (PGZ 301) potentiostat/galvanostat was used to perform the impedance spectroscopy studies. Impedance measurements were carried out in the frequency range 100 k–100 mHz. The working electrode was first maintained in the test environment for 30 min to reach an equilibrium state before the impedance run. This served to put the electrode in a reproducible initial state and to make sure that no blistering occurred during the conditioning period. All experiments were performed at a room temperature of 25 ± 0.5°C. All data were repeated at least three times to ensure reproducibility and statistical significance.

Preparation of free-standing films and barrier property measurements

Typically, the 3 mL of PIC5% solution was cast onto a substrate (e.g., a microscope glass slide). The NMP solvent was allowed to evaporate at 150°C in an oven for 15 h. The sample-coated glass substrate was then immersed in distilled water at 70°C for 2 h to give the film of PIC5% materials. The same procedure was used to synthesize neat PI, PIS5% and PISC2.5% membranes. Oxygen permeability of membrane is determined by using the Yanco GTR-10 gas permeability analyzer. Gas permeability is calculated by the following equation:

$$P = l/(p_1 - p_2) \times (q/t)/A$$

where P is the gas permeability [cm^3(STP)$(cm/cm^2)^{-1}$ $(s)^{-1}$ $(cmHg)^{-1}$]; q/t is the volumetric flow rate of the gas permeate [cm^3(STP)s^{-1}]; l is the free-standing film thickness [cm]; A is the effective free-standing film area [cm^2]; and p_1 and p_2 are the pressures [cmHg] on the high-pressure and low-pressure sides of the free-standing film, respectively. The rate of transmission of O_2 was obtained by gas chromatography, from which the air permeability was calculated. On the other hand, experiment of H_2O permeability performed by apparatus similar to our previous published article.[23,24] The feed solution is not in contact with the membrane. The feed solution is vaporized first and subsequently permeated through the membrane with an effective area of about 10.2 cm^2. The permeation rate is determined by measuring weight of permeate.

RESULTS AND DISCUSSIONS

Characterization

The representative FTIR spectra of organophilic clay, intercalating agent, and montmorillonite (MMT) clay

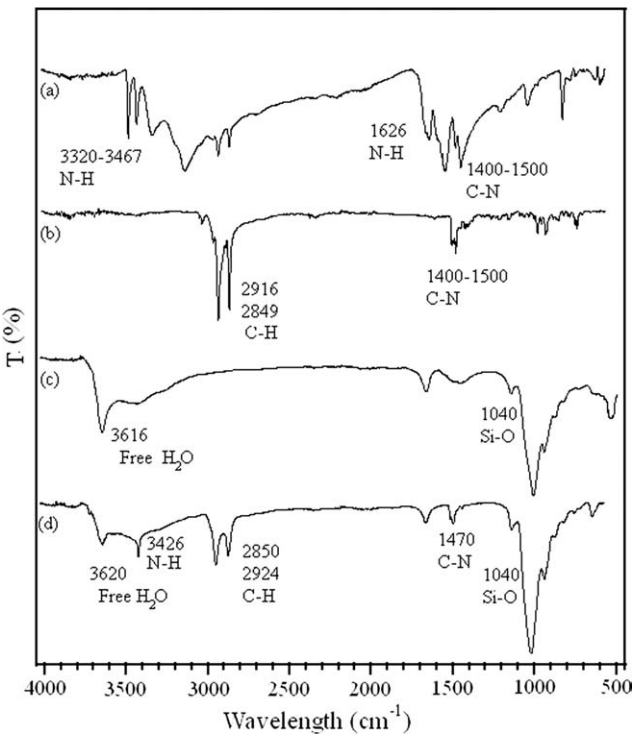

Figure 1 Representative FTIR spectra of (a) melamine, (b) HTAB, (c) Na+−MMT, and (d) organophilic clay.

are shown in Figure 1. The characteristic absorption bands of melamine are shown at 3320–3467 and 1626 cm^{-1}(N—H stretching), 1400–1500 cm^{-1}(C—N stretching). The characteristic absorption bands of HTAB appear 2916, 2849 cm^{-1}(C—H stretching) and 1400–1500 cm^{-1}(C—N stretching), as shown in Figure 1(a,b). The characteristic vibration bands of MMT clay are found at 1040 cm^{-1} (Si—O),[24,25] as shown in Figure 1(c). Furthermore, the characteristic bands of organophilic clay are shown in Figure 1(d), which displays organophilic clay at 3426 cm^{-1}(N—H stretching), 2924 and 2850 cm^{-1}(C—H stretching), 1470 cm^{-1}(C—N stretching) and 1040 cm^{-1} (Si—O), shown the intercalating agent was intercalated into the silicate layers. Figure 2 shows the FTIR spectra of neat PI, PIS5%, PIC5%, and PISC2.5% materials. As the loading of 5 wt % silica (PIS5%), the characteristic vibration bands of silica was found at 960 cm^{-1} (Si—OH).[26,27] Furthermore, the PISC2.5% was found the characteristic vibration of MMT clay at 1040 cm^{-1} (Si—O), as shown in Figure 2(d). When the loading of organophilic clay is increased to 5 wt % (e.g., PIC5%), the intensity of MMT clay bands became more pronounced in Figure 2(c).

Figure 3 shows the wide-angle powder X-ray diffraction patterns of MMT, organophilic clay, PIC5% and PISC2.5% materials. There is a peak appearing for organophilic clay at $2\theta = 4.1°$ (d-spacing = 21.5 nm), as opposed to the diffraction peak at $2\theta = 6.8°$ (d-spacing = 12.9 nm) for MMT clay. For Figure

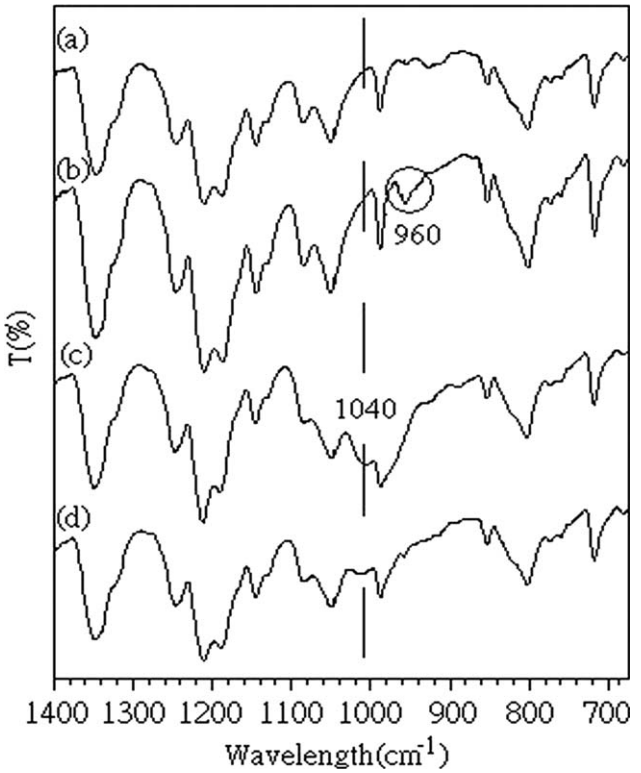

Figure 2 Representative FTIR spectra of (a) PI, (b) PIS5%, (c) PIC5%, and (d) PISC2.5%.

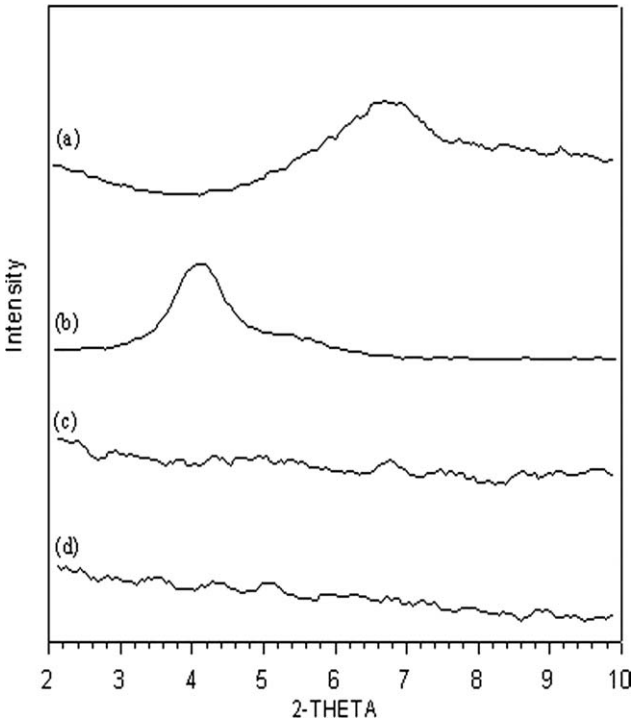

Figure 3 Wide-angle powder X-ray diffraction patterns of (a) Na+−MMT, (b) organophilic clay, (c) PIC5%, and (d) PISC2.5%.

3(c,d), there is a lack of any diffraction peak in $2\theta = 2$–10° as opposed to the diffraction peak at $2\theta = 4.1^\circ$ (*d* spacing 21.5 nm) for organophilic clay, indicating the possibility of having exfoliated silicate layers of organophilic clay dispersed in the PI material.[28,29]

Figure 4 shows the NMR spectroscopy. Solid-state ^{29}Si NMR spectroscopy is powerful method for characterizing the chemical structure of the SiO_2 prepared from TEOS. Solid-state ^{29}Si NMR spectroscopy provides quantitative information about the condensation reaction. Solid-state ^{29}Si NMR spectra of the PIS5% are shown in Figure 4. The peaks at −101 and −110 ppm in ^{29}Si NMR spectra of the PIS5% were assigned to fully condensed Q^3 and Q^4 species, respectively.[9] Q^1 and Q^2 peaks were too small to be analyzed in the spectra. The formation of Q^1 and Q^2 species was insignificant, suggesting that no unreacted TEOS monomer was present. The dispersion of SiO_2 into polyimide was obtained from the TEM.

The morphology studies for dispersion capability of silica particle and organophilic clay in PI matrix can be observed through the observation of transmission electron microscopy (TEM), as shown in Figure 5. For example, TEM micro-image for PIC5% showed morphology of exfoliated (major) and intercalated (minor) structures, as shown in Figure 5(a). The dispersion of SiO_2 into polyimide was obtained from Figure 5(b). Observed Figure 5(a,b), the clay average length is 688 nm and the silica particle average diameter is 438 nm and, besides, the aspect ratio of clay is higher than silica a lot. When the silica particle and the organophilic clay are simultaneously appear in the PI matrix, as shown in Figure 5(c),

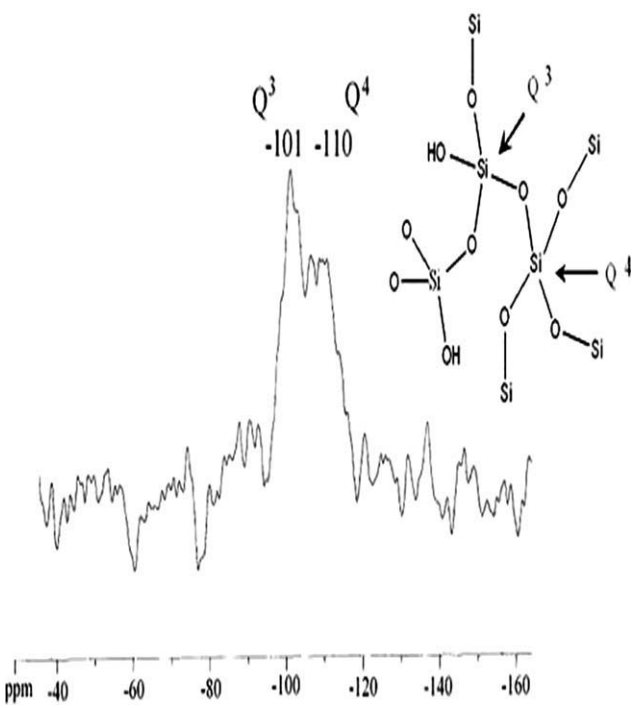

Figure 4 29Si solid-state NMR spectrum of PIS5%.

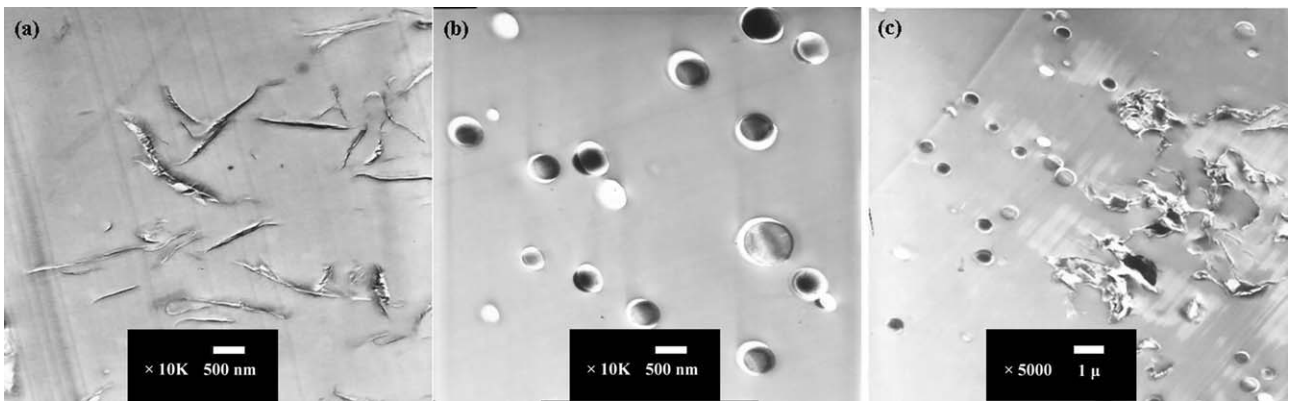

Figure 5 TEM micrographs for (a) PIC5% at ×10,000, (b) PIS5% at ×10,000, and (c) PISC2.5% at ×5,000.

which is similar to those obtained from the polyacrylonitrile composites containing Na^+-montmorillonite and SiO_2 particle reported by Yu et al.[30] Thank's for the reviewer's suggestion. The TEM of PISC2.5% shown in Figure 5(c) seem to reveal more intercalate can be explained as follows. The dispersion of clay platelets may considerably be effected by the incorporation of TEOS. Sol–Gel reactions of TEOS occurred in composites leading to the formation of three-dimensional networks of Si—O—Si linkage would significantly increase shear viscosity of entire solution, which may significantly effect the dispersion of clay platelets in polymer matrix, leading to a mainly intercalated structure of clay.[31–33] Moreover, we also cited that the related literatures that reviewer mentioned.

Potentiodynamic measurements

In this section, corrosion protection effect on the CRS electrodes coated with as-prepared PI, PIS, PIC, and PISC can be evaluated by operating sequential electrochemical corrosion parameters such as E_{corr}, R_p, i_{corr}, and corrosion rate (R_{corr}).

Generally, CRS electrodes coated with neat PI coating shows a higher E_{corr} value than the uncoated CRS electrode, which is consistent with previous observation on organic-based coating system.[34] However, it revealed a lower E_{corr} value than the specimen coated. For example, PIS5%-coated CRS electrode exhibited a high corrosion potential of ca. –644 mV at running time of 30 min (I_{corr} = 8.12 μA/cm^2). Even after 5 h measurement, the potential remained at ca. –648 mV. Such E_{corr} value implies that the PIS5%-coated CRS electrode is noble towards the electrochemical corrosion compared to the neat PI (ca. – 655mV). Furthermore, the PIC5%-coated CRS showed corrosion potential of –551 mV (I_{corr} = 1.97 μA/cm^2), which is significantly lower than PIS5%, indicating that PIC5% display better corrosion protection performance on CRS electrode than that of PI and PIS5%. The most anodic value of E_{corr} indicates that the PIC5%-coated CRS electrode should have the highest corrosion protection. Therefore, this shift is related to transformation of emeraldine state of PIC5% coating to the leucoemeraldine state corrosive solutions.[35] The polarization resistances, R_p, were evaluated from the Tafel plots, according to the Stearn-Geary equation.[36]

$$R_p = b_a b_c / 2.303(b_a + b_c) I_{corr}$$

Here, I_{corr} is the corrosion current determined by an intersection of the linear portions of the anodic and cathodic curves, and b_a and b_c are anodic and cathodic Tafel slopes ($\Delta E/\Delta \log I$), respectively. The protection efficiency (P_{EF} %) values were estimated using the following equation[37]:

$$P_{EF}\,\% = 100[R_p^{-1}(\text{uncoated}) - R_p^{-1}(\text{coated})]/R_p^{-1}(\text{coated}).$$

The CRS electrodes coated with PIC5% showed a polarization resistance (R_p) value of 59.63 kΩ cm^2 in 5 wt % NaCl electrolyte, which is obviously greater than that of CRS electrode coated with PIS5% (R_p = 19.06 kΩ cm^2). Tafel plot for (a) bare, (b) PI-coated, (c) PIS5%-coated, (d) PISC2.5-coated, (e) PIC5%-coated CRS electrodes are shown in Figure 6. For example, the corrosion current (i_{corr}) of CRS electrode coated with PIC5% is *ca.* 1.97 μA/cm^2, which is correspondent to a corrosion rate (R_{corr}) of *ca.* 0.027 milliinches per year (MPY), which is significantly lower than that of PIS5% (i.e., 9.6 μA/cm^2 and 0.113 MPY), as summarized in Table I.

Electrochemical impedance measurements

Electrochemical impedance spectroscopy (EIS) was an alternative tool to evaluate the activity difference between CRS surface after neat PI and PISC material treatment. Impedance is a totally complex resistance

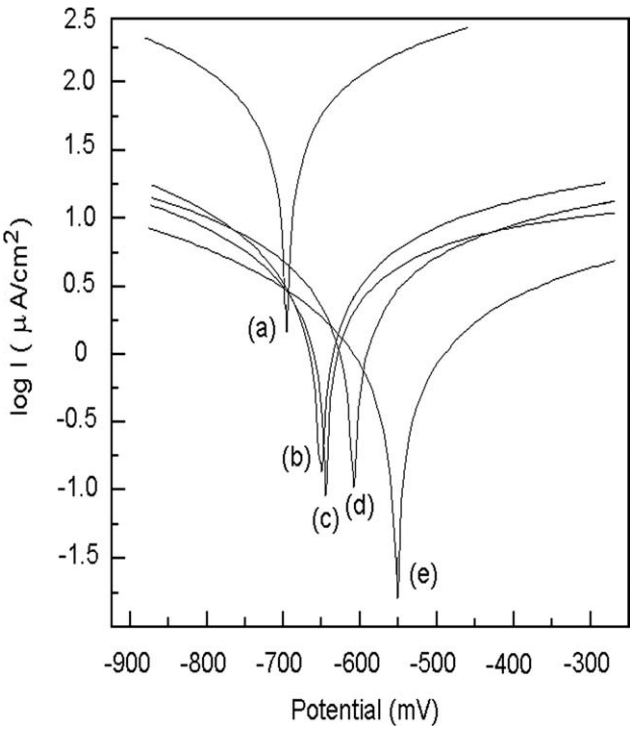

Figure 6 Tafel plots for (a) Bare, (b) PI-coated, (c) PIS5%-coated, (d) PISC2.5%-coated, and (e) PIC5%-coated CRS measured in 5 wt % NaCl aqueous solution.

when a current flows through a circuit made of capacitors, resistors, or insulators, or any combination of these.[38] EIS measurement results in currents over a wide range in frequency. For organic coating systems, the equivalent circuit simulating EIS results in Figure 7(a) is well accepted. The impedance (Z) depends on the charge transfer resistance (R_{ct}), the solution resistance (R_s), the coating pore resistance (R_{po}), the capacitance of the intact coating (C_c), the capacitance of the electrical double layer or oxide film capacitance (C_{dl}), and the current frequency of the AC signal (ω). For intact coatings, the coating resistance R_{po} is much higher compared with the electrochemical reaction parameters.[39] Supposing the solution resistance R_s is negligible, during the early period of immersion, the equivalent circuit shown in Figure 7(a) may be approximately expressed as a parallel connection of R_{po} and C_c, the impedance of which can be reduced as[40,41]:

$$Z = R_{po}/1 + (\omega C_c R_{po})^2 - j(\omega C_c R_{po}{}^2)/1 + (\omega C_c R_{po})^2$$

The high-frequency intercept is equal to the solution resistance, and the low-frequency intercept is equal to the sum of the solution and charge transfer resistances.[42] The higher the semicircle diameter (charge transfer resistance) indicated the lower the corrosion rate.[43] In this study, four samples were prepared. The first sample (a′) was neat PI-coated CRS. A series of samples denoted with (b′)–(d′) were coated by PISC materials with different content of silica particle and organophilic clay loading. The corrosion protection studies of these samples with about 30 ± 2 μm in coating thickness immersed in 5 wt % aqueous NaCl electrolyte for 30 min was followed by EIS. The lower part of Figure 7(b) shows the Nyquist plots of the four samples. First of all, we found that the charge transfer resistance of samples as determined by the intersection of the low frequency end of the semicircle arc with the real axis is 75, 385, 830, and 1750 KΩ cm^2, respectively. This result clearly demonstrated that the sample, with the highest organophilic clay loading up to 5 wt %, has the greatest corrosion protection performance.

Furthermore, EIS Bode plots (impedance vs. frequency) of PISC materials samples loaded with various content of organophilic clay are shown in Figure 8. The increase of impedance value at high clay loading in the monitoring frequency region from low to high frequency can be interpreted due to the barrier effect of organophilic clay dispersing in PISC composites. Again, PIC5%, exhibited a higher charge resistance than that of PIS5%, in the entire monitoring frequency range based on the studies of EIS Bode plots. In conclusion, the enhanced barrier effect in PISC materials, in the form of coating, compared to neat PI might be resulted from the effectively dispersing of organophilic clay platelets and silica particle in PI matrix to further increase the tortuosity of diffusion pathway of H_2O and O_2 molecules. This is

TABLE I
Relations of the Composition of Polyimide-Silica-Clay Composite Materials with E_{corr}, R_p, I_{corr}, and R_{corr} Measured from Electrochemical Methods

	Feed composition (wt %)			Electrochemical corrosion measurements					
Compound code	PI	Clay	Silica	E_{corr} (mV)	R_p (kΩ cm^2)	I_{corr} (μA/cm^2)	R_{corr} (MPY)	Thickness (μm)	P_{EF} (%)
Bare	–	–	–	−695	1.33	22.90	8.820	–	–
PI	100	0	0	−655	15.41	9.67	0.113	30	10.58
PIS5%	95	0	5	−644	19.06	8.12	0.094	31	13.33
PISC2.5%	95	2.5	2.5	−606	20.47	6.96	0.082	30	14.39
PIC5%	95	5	0	−551	59.63	1.97	0.027	29	43.83

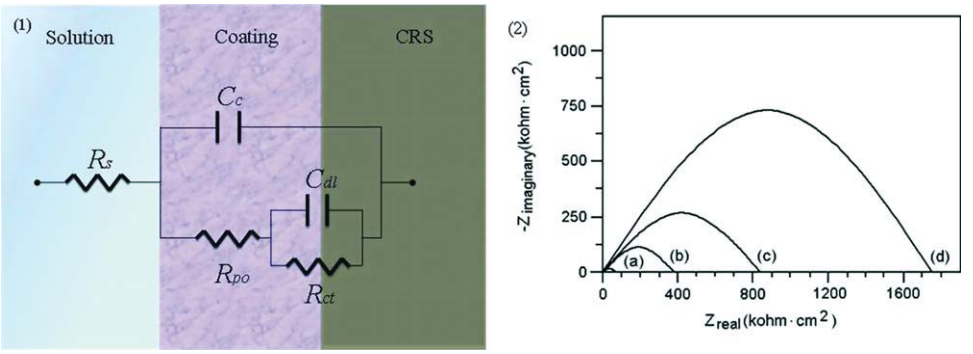

Figure 7 Analog circuit (a) and Nyquist plots (b) for (a′) PI-coated, (b′) PIS5%-coated, (c′) PISC2.5%-coated, and (d′) PIC5%-coated CRS measured in 5 wt % NaCl aqueous solution. [Color figure can be viewed in the online issue, which is available at wileyonlinelibrary.com.]

further evidenced by the studies of the gas permeability studies as discussed in the following section.

Gas permeability measurements

The free-standing film of neat PI and PISC materials used for the evaluation of molecular barrier properties were prepared to have film (thickness of ~ 100 μm). Compared with neat PI film, PIS5% shows about ~ 4% and ~ 24% reduction in O_2 and H_2O permeability, as shown in Figure 9. The reduction in gas permeability may probably be associated with the barrier properties of the grain of silica particle effectively dispersed in the PI matrix. Furthermore, PISC2.5% film showed an obvious reduction in the barrier of O_2 and H_2O molecules as compared to that of PIS5%, which may be resulted from that the platelets of organophilic clay, display a better barrier in PI matrix relative to grain of silica particle. When the amount of organophilic clay was increased to 5 wt %, there was about 30% and 55% reduction in O_2 and H_2O permeability than neat PI, respectively.

Optical clarity of PISC films

Figure 10 shows the UV-visible transmission spectra of neat PI and a series of PISC materials films. These films have film thickness of about 100 μm. The

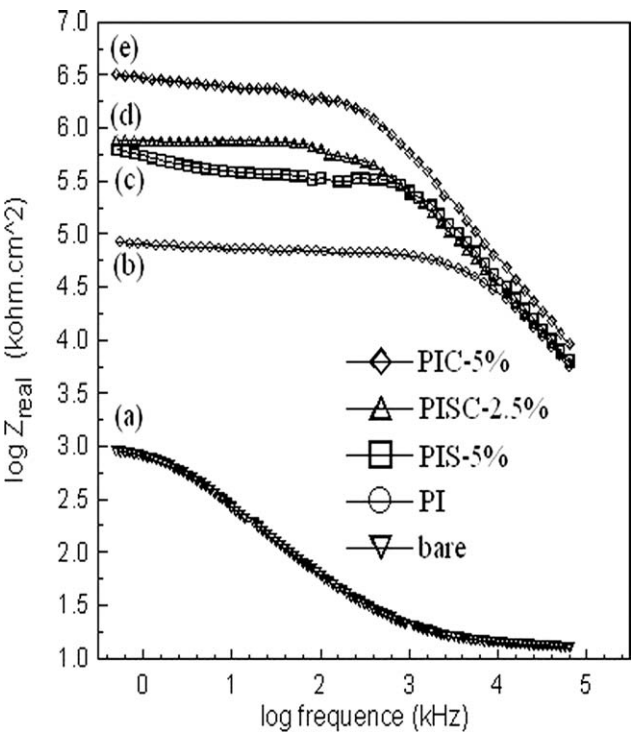

Figure 8 Bode plots for (a) Bare, (b) PI-coated, (c) PIS5%-coated, (d) PISC2.5%-coated, and (e) PIC5%-coated CRS measured in 5 wt % NaCl aqueous solution.

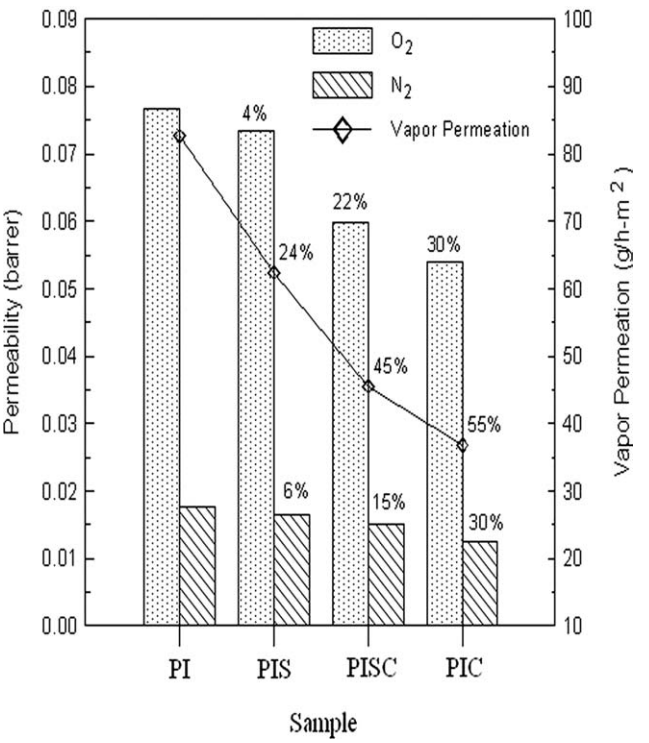

Figure 9 H_2O and O_2/N_2 permeability as a function of PI, PIS5%, PISC2.5%, and PIC5%.

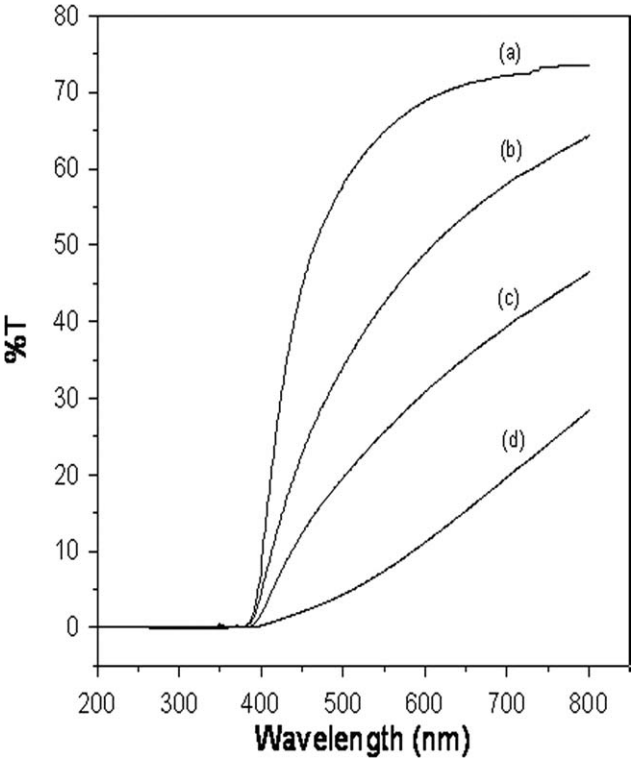

Figure 10 UV-visible transmission spectra of (a) PI, (b) PIS5%, (c) PISC2.5%, and (d) PIC5%.

transmission spectra of neat PI membranes in the visible light regions (400–700 nm) are slightly affected by the presence of the 5 wt % silica particle loading in the PIS5% membranes. However, the spectra of as-prepared membrane at higher clay loading (e.g., PIC5%) exhibits lower optical clarity, reflecting that there is strong scattering of clay resulting in lower transparency of the UV–visible light.[25]

DISCUSSION

In this study, we present the anticorrosion properties of polyimide-silica-clay composite. The anticorrosion properties of PIC and PIS have been published before. Till now, no literature has reported the anticorrosion properties of clay and the particles exist in same system. A series of materials that consist of PI, silica particle, and layered montmorillonite (MMT) clay are prepared by effectively dispersing method. In PISC system, the total material loadings are maintained at 5%. For comparison, the results obtained for neat PI, PIS, PIC, and PISC are also included. The corrosion potential (E_{corr}), polarization resistance (R_p) of PIC are higher than that of neat PI. The O_2/H_2O gas barrier properties of PIC5% system are considerably better than that of PIS5% and PISC2.5%. With changing the SiO_2/clay weight ratio from 5 : 0 to 2.5 : 2.5 and 0 : 5, the E_{corr} and R_p value increase. The H_2O gas barrier properties of PIC5% is 55% higher than that of neat PI, 31% and 10% higher than those of PIS5% and PISC2.5%, respectively. The reason may probably be attributed to the aspect ratio of layered clay which is higher than SiO_2. The H_2O and O_2 molecules usually cause metal substance to oxidize. Increasing the clay ratio in polymer would increase the length of diffusion pathway of H_2O and O_2 molecules. In PISC system, the predominant reason for corrosion protection is clay loading. Increasing the clay ratio in PI material will improve the value of corrosion potential (E_{corr}), polarization resistance (R_p), and decrease value of corrosion current (i_{corr}), and corrosion rate (R_{corr}).

References

1. Tyan, H. L.; Liu, Y. C.; Wei, K. H. Chem Mater 1999, 11, 1942.
2. Wang, Z.; Pinnavaia, T. J. 1998, 10, 3769.
3. Lan, T.; Kaviratna, P. D.; Pinnavaia, T. J. Chem Mater 1994, 6, 573.
4. Chang, K. C.; Lai, M. C.; Peng, C. W.; Chen, Y. T.; Yeh, M. J.; Lin, C. L. Acta Mater 2006, 51, 5645.
5. Gilman, W. J.; Jackson, C. L.; Morgan, A. B.; Jr, R. H. Chem Mater 2000, 12, 1866.
6. Yeh, J. M.; Liou, S. J.; Lai, C. Y.; Wu, P. C. Chem Mater 2001, 13, 1131.
7. Yeh, J. M.; Liou, S. J.; Lin, C. Y.; Cheng, C. Y.; Chang, Y. W. Chem Mater 2002, 14, 154.
8. Yu, Y. H.; Yeh, J. M.; Liou, S. J.; Chang, Y. P. Acta Mater 2004, 52, 475.
9. Brinker, C. J.; Scherer, G. W. Sol-Gel Science: The Physics and Chemistry of Sol-Gel Processing; Academic Press, 1990; Chapter 1.
10. Kato, K. J Mater Sci 1992, 27, 1445.
11. Kato, K. J Mater Sci 1993, 28, 4033.
12. Frings, S.; Meinema, H. A.; Van Nostrum, C. F.; Vander-Linde, R. Prog Org Coat 1998, 33, 126.
13. Messadeq, S. H.; Pulcinelli, S. H.; Santilli, C. V.; Guastaldi, A. C.; Messadecq, Y. J. Non-Cryst Solids 1999, 247, 164.
14. Yeh, M. J.; Chin, C. P.; Chang, S. J Appl Polym Sci 2003, 88, 3264.
15. Yeh, J. M.; Chen, C. L.; Chen, Y. C.; Ma, C. Y.; Lee, K. R.; Wei, Y.; Li, S. Polymer 2003, 43, 2729.
16. Morgan, A. B.; Gilman, J. W.; Jackson, C. L. Macromolecules 2001, 34, 2735.
17. Agag, T.; Koga, T.; Takeichi, T. Polymer 2001, 42, 3399.
18. Gu, A.; Kuo, S. W.; Chang, F. C. J Appl Polym Sci 2001, 79, 1902.
19. Huang, J. C.; Zhu, Z. K.; Yin, J.; Qian, X. F.; Sun, Y. Y. Polymer 2001, 42, 873.
20. Gu, A.; Chang, F. C. J Appl Polym Sci 2001, 79, 289.
21. Yeh, J. M.; Hsieh, C. F.; Jaw, J. H.; Kuo, T. H.; Huang, H. Y.; Lin, C. L.; Hsu, M. Y. J Appl Polym Sci 2005, 95, 1082.
22. Hsiao, S. H.; Liou, G. S.; Chang, L. M. J Appl Polym Sci 2001, 80, 2067.
23. Huang, C. C.; Jang, G. W.; Chang, K. C.; Hung, W. I.; Yeh, J. M. Polym Int 2008, 57, 605.
24. Yeh, J. M.; Yu, M. Y.; Liou, S. J. J Appl Polym Sci 2003, 89, 3632.
25. Yua, Y. H.; Lina, C. Y.; Yeha, J. M.; Lin, W. H. Polymer 2003, 44, 3553.
26. Chiu, Y. C.; Ma, C. C.; Liu, F. Y.; Chiang, C. L.; Riang, L.; Yang, J. C. Eur Polym J 2008, 44, 1003.

27. Lu, Q.; Chen, D.; Jiao, X. Chem Mater 2005, 17, 4168.
28. Liu, H.; Han, C.; Dong, L. J Appl Polym Sci 2009, 115, 3120.
29. Chakraborty, S.; Kar, S.; Dasgupta, S.; Mukhopadhyay, R.; Bandyopadhyay, S.; Joshi, M.; Ameta, S. C. J Appl Polym Sci 2009, 116, 1660.
30. Yu, T.; Lin, J.; Xu, J.; Chen, T.; Lin, S. Polymer 2005, 46, 5695.
31. Huang, S. L.; Chin, W. K.; Yang, W. P. J Polym Sci B Polym Phys 2004, 42, 3476.
32. Lim, S. T.; Hyun, Y. H.; Choi, H. J. Chem Mater 2002, 14, 1839.
33. Hyun, Y. H.; Lim, S. T.; Choi, H. J.; Jhon, M. S. Macromolecules 2001, 34, 8084.
34. Huang, K. Y.; Jhuo, Y. S.; Wua, P. S.; Lin, C. H.; Yu, Y. H.; Yeh, J. M. Eur Polym J 2009, 45, 485.
35. Yağan, A.; Pekmez, N. Ö.; Yıldız, A. Electrochim Acta 2008, 53, 5242.
36. Stern, M.; Geary, A. L. J Electrochem Soc 1957, 104, 56.
37. Bockris, J.; Reddy, K. N. Modern Electrochemistry; Wiley: New York, 1976.
38. Park, S. M.; Yoo, J. S. Anal Chem 2003, 75, 455A.
39. Grundmeier, G.; Schmidt, W.; Stratmann, M. Electrochim Acta 2000, 45, 2515.
40. Zuo, Y.; Pang, R.; Li, W.; Xiong, J. P.; Tang, Y. M. Corros Sci 2008, 50, 3322.
41. Martinez, S.; Žulj, L. V.; Kapor, F. Corros Sci 2009, 51, 2253.
42. Amirudin, A.; Thierry, D. Prog Org Coat 1995, 26, 1.
43. Medrano-Vaca, M. G.; Gonzalez-Rodriguez, J. G.; Nicho, M. E.; Casales, M. Electrochim Acta 2008, 53, 3500.